Title

Redox-dependent gating of VDAC by mitoNEET.

Journal

Proceedings of the National Academy of Sciences of the United States of America, 116(40)

ISSN

0027-8424

Authors

Lipper, Colin H
Stofleth, Jason T
Bai, Fang
et al.

Publication Date

2019-10-01

DOI

10.1073/pnas.1908271116

Peer reviewed

Redox-dependent gating of VDAC by mitoNEET

Colin H. Lipper[a,1], Jason T. Stofleth[a,1], Fang Bai[b,c,d,e], Yang-Sung Sohn[d], Susmita Roy[b,c,d,e], Ron Mittler[g,h], Rachel Nechushtai[f], José N. Onuchic[b,c,d,e,2], and Patricia A. Jennings[a,2]

[a]Department of Chemistry and Biochemistry, University of California San Diego, La Jolla, CA 92093-0375; [b]Center for Theoretical Biological Physics, Rice University, Houston, TX 77005; [c]Department of Physics and Astronomy, Rice University, Houston, TX 77005; [d]Department of Chemistry, Rice University, Houston, TX 77005; [e]Department of Biosciences, Rice University, Houston, TX 77005; [f]The Alexander Silberman Institute of Life Science, The Hebrew University of Jerusalem, Jerusalem 91904, Israel; [g]Department of Surgery, University of Missouri School of Medicine, Columbia, MO 65201; and [h]Christopher S. Bond Life Sciences Center, University of Missouri, Columbia, MO 65201

Contributed by José N. Onuchic, August 19, 2019 (sent for review May 14, 2019; reviewed by Maurizio Pellecchia and Sichun Yang)

MitoNEET is an outer mitochondrial membrane protein essential for sensing and regulation of iron and reactive oxygen species (ROS) homeostasis. It is a key player in multiple human maladies including diabetes, cancer, neurodegeneration, and Parkinson's diseases. In healthy cells, mitoNEET receives its clusters from the mitochondrion and transfers them to acceptor proteins in a process that could be altered by drugs or during illness. Here, we report that mitoNEET regulates the outer-mitochondrial membrane (OMM) protein voltage-dependent anion channel 1 (VDAC1). VDAC1 is a crucial player in the cross talk between the mitochondria and the cytosol. VDAC proteins function to regulate metabolites, ions, ROS, and fatty acid transport, as well as function as a "governator" sentry for the transport of metabolites and ions between the cytosol and the mitochondria. We find that the redox-sensitive [2Fe-2S] cluster protein mitoNEET gates VDAC1 when mitoNEET is oxidized. Addition of the VDAC inhibitor 4,4′-diisothiocyanatostilbene-2,2′-disulfonate (DIDS) prevents both mitoNEET binding in vitro and mitoNEET-dependent mitochondrial iron accumulation in situ. We find that the DIDS inhibitor does not alter the redox state of MitoNEET. Taken together, our data indicate that mitoNEET regulates VDAC in a redox-dependent manner in cells, closing the pore and likely disrupting VDAC's flow of metabolites.

VDAC1 | mitoNEET | CISD1 | direct coupling | ferroptosis

The NEET family of [2Fe-2S] proteins plays essential roles in the regulation of mitochondrial iron and reactive oxygen species (ROS) homeostasis, as well as in the activation of apoptosis, ferroptosis, and autophagy (1–3). NEET proteins are associated with several human pathologies including diabetes, cancer, neurodegeneration, Parkinson's disease, Wolfram syndrome 2, and cystic fibrosis (4–9). Many of these pathologies display various degrees of mitochondrial dysfunction, for which mitoNEET (mNT) is a critical regulator (10, 11). NEET proteins contain a signature CDGSH domain and are highly conserved from archaea to humans (12–14). Each CDGSH domain binds to a redox-active [2Fe-2S] cluster via a characteristic 3Cys-1His coordination motif (15, 16). There are 3 human members of the family, mitoNEET (mNT, *CISD1*), NAF-1 (ERIS, Miner1, *CISD2*), and MiNT (Miner2, Melanoma nuclear protein 13, *CISD3*). The founding member of the NEET family, mNT, is a homodimer localized to the cytosolic side of the outer-mitochondrial membrane (OMM) by a single-pass N-terminal α-helix per protomer. In addition, each protomer coordinates a single [2Fe-2S] cluster (16–18). Interestingly, mNT can repair the [4Fe-4S] cluster of cytosolic iron-regulatory protein 1 (IRP1/aconitase), an important regulator of iron metabolism by either transferring Fe or [2Fe-2S] clusters to it (19). Mitochondrial-associated mNT also efficiently transfers its [2Fe-2S] clusters to apo-acceptor proteins such as the CIA important protein anamorsin (or ciapin1), an electron transfer protein involved in the assembly of cytosolic Fe-S clusters (16, 20–22). Although mNT is able to donate its [2Fe-2S] clusters to apo-acceptor proteins, it remains unclear how mNT is able to exchange Fe-S clusters with the mitochondria.

VDAC actively governs mitochondrial metabolism and function through interaction-based gating (23, 24). VDAC plays a central role in neurodegenerative diseases (e.g., Alzheimer's disease) (25–29) and destructive processes (e.g., ROS accumulation) (30–33), as well as regulates apoptotic functions in the cell (24). mNT's placement at the OMM with a redox-sensitive domain suggests that it could be an excellent candidate to modulate the activity of VDAC. Humans have 3 VDAC paralogs encoded by 3 separate genes (*VDAC1*, *VDAC2*, and *VDAC3*) (34, 35), and mNT was identified as an interaction partner with all 3 forms in multispecies cofractional investigations (36, 37). In this study, we focus on VDAC1 as it is the most abundant channel in the mitochondrial membrane, and controls mitochondrial respiration as well as transports diverse metabolites and ions (other than the eponymous anions) between the cytosol and the intermembrane space (23, 38, 39). VDAC controls passage of metabolites between the cytosol and mitochondrial intermembrane space via modulation of different open and closed states of the protein (40). VDAC1 expression level is controlled independently of the expression level of VDAC2 and VDAC3 (41). Therefore, in this study, we characterize the effect of VDAC1 (hereafter referred to as VDAC) interactions with mNT.

Our studies indicate that mNT regulates the channel function of VDAC and that this interaction is dependent on the redox state of mNT's [2Fe-2S] clusters. Additionally, using a combination of hydrogen–deuterium exchange mass spectrometry (HDX-MS) and computational docking methodologies, we identify the protein–protein interaction regions involved in the association

Significance

This work demonstrates that the outer mitochondrial-anchored [2Fe-2S] mitoNEET is able to bind within the central cavity of the voltage-dependent anion channel (VDAC) and regulate its gating in a redox-dependent manner. These findings have implications for ferroptosis, apoptosis, and iron metabolism by linking VDAC function, mitoNEET, and the redox environment of the cell. Furthermore, these findings introduce a potential player to the many mechanisms that may alter VDAC's governance in times of homeostasis or strife.

Author contributions: R.M., R.N., J.N.O., and P.A.J. designed research; C.H.L., J.T.S., F.B., Y.-S.S., S.R., R.N., and P.A.J. performed research; C.H.L., J.T.S., F.B., Y.-S.S., S.R., R.M., J.N.O., and P.A.J. analyzed data; and C.H.L., J.T.S., R.M., R.N., J.N.O., and P.A.J. wrote the paper.

Reviewers: M.P., University of California, Riverside; and S.Y., Case Western Reserve University.

The authors declare no conflict of interest.

[1]C.H.L. and J.T.S. contributed equally to this work.

[2]To whom correspondence may be addressed. Email: jonuchic@rice.edu or pajennings@ucsd.edu.

This article contains supporting information online at www.pnas.org/lookup/suppl/doi:10.1073/pnas.1908271116/-/DCSupplemental.

First published September 16, 2019.

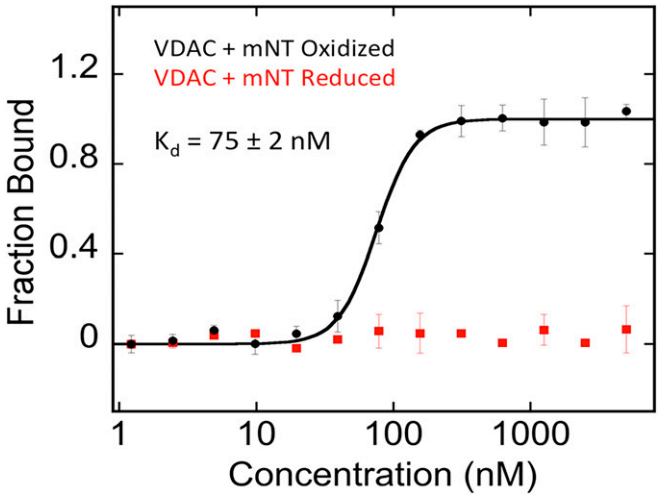

Fig. 1. mNT binding to VDAC is redox state dependent. MST analysis used to assess the affinity of mNT to fluorescently labeled VDAC reconstituted in 1% DMPC/CHAPSO bicelles under oxidizing conditions results in measured K_d of 76 ± 2 nM (black). When mNT is reduced with DTT, binding is not observed (red).

between mNT and VDAC. Importantly, we demonstrate that the VDAC inhibitor 4,4′-diisothiocyanatostilbene-2,2′-disulfonate (DIDS), which blocks VDAC via an initial reversible reaction followed by irreversible cross-linking (42, 43), abrogates the binding of mNT to VDAC in vitro and also prevents mNT from transferring its Fe/[2Fe-2S]s in situ. In addition, DIDS does not alter the redox state of mNT. Taken together, our results underscore the relevance of the redox-dependent interaction between mNT and VDAC in maintaining cellular homeostasis and the regulation of Fe and [2Fe-2S] clusters in cells.

Results and Discussion

High Affinity and Redox Modulation of VDAC–mNT Interaction. Microscale thermophoresis (MST) was employed to quantify the affinity of the VDAC–mNT interaction. Fluorescently labeled human VDAC in dimyristoyl phosphatidylcholine (DMPC)/3-[(3-cholamidopropyl) dimethylammonio]-2-hydroxy-1-propanesulfonate (CHAPSO) bicelles (1% final concentration) was incubated with increasing concentrations of mNT and analyzed by MST, and a dissociation constant (K_d) of 76 ± 2 nM of mNT for VDAC was determined (Fig. 1). Reduction with dithiothreitol (DTT) prevented any detectable binding of mNT to VDAC, indicating that mNT binds to VDAC when its [2Fe-2S] clusters are oxidized (e.g., when the protein or lysates are exposed to oxygen; Fig. 1). The dependency of the interaction of mNT–VDAC on the oxidation state of mNT suggests that it may be part of a response to oxidative stress, as the redox-active mNT is typically in a reduced state under normal cellular conditions (44, 45). Due to its redox potential ($E_{m,7}$) of +30 mV, mNT can be oxidized under conditions such as cell stress in disease states, defense, or cell death (46, 47).

The VDAC channel adopts a high-conductance "open" state, as well as several low-conductance "closed" states. When VDAC adopts a closed conformation (48), it inhibits ATP flux across the channels. In addition, VDAC channel permeability is regulated by binding to Bcl2 family proteins, hexokinase and tubulin (48–50). As mNT interacts with both proapoptotic and antiapoptotic proteins in the BCL family, we explored the role of mNT in regulating VDAC function. VDAC conductance was recorded both in the absence and presence of mNT across a range of applied voltages. The characteristic VDAC voltage-dependent conductance pattern is observed in the absence of added mNT protein, with decreasing conductance as voltage is increased above ~35 mV (both positive and negative), as expected (40, 51) (Fig. 2). In the presence of mNT, the observed channel conductance is significantly inhibited across the entire voltage spectrum as compared to that observed in the absence of added protein (Fig. 2). In contrast, the presence of NAF-1, a related NEET protein, had a smaller effect on the conductance changes across the voltage range, and this protein may have a separate function associated with the truncated VDAC-ΔC form (19).

Structural Analysis of the VDAC–mNT Interaction. We utilized HDX-MS to interrogate the interaction interface between mNT and VDAC. Backbone amide protons in both proteins provide probes for interactions as they can be protected from exchange with the solvent at the binding interface, as well as cause changes in deuterium exchange rates at sites distal to the binding interface (52). Analyzing the monomeric VDAC–nanodisc complex (VDAC–cND) allowed us to investigate affects arising solely from the interaction of VDAC with mNT. MST binding analysis indicates that oxidized mNT binds to VDAC with a K_d of 210 ± 15 nM (*SI Appendix*, Fig. S1). In order to interrogate the protein–protein interface, protease digestion after defined time periods of HD exchange with interaction were performed. Digestion of mNT produces 125 peptide probes and high (89%) sequence coverage. Digestion of the integral membrane protein VDAC also results in high sequence coverage, with a total of 91 peptide probes covering this integral membrane protein. Comparative heat map representations of the hydrogen–deuterium exchange kinetics of apo and complexed mNT and VDAC are provided in *SI Appendix*, Figs. S2 and S3. Deuterium incorporation plots for representative peptide probes within regions that display significant changes in protection upon complex formation are shown for both mNT and VDAC. The regions displaying changes in exchange protection are highlighted on the respective protein structures in Figs. 3 and 4. The regions of mNT with increased protection upon complex formation include the [2Fe-2S] cluster-binding region, the strand swapped outer β-strand, and the α-helix within the cluster binding domain (16). VDAC protection increases at loop regions on the cytosolic side of the pore, with 3 consecutive loops on the C-terminal end of the barrel and 1 loop juxtaposed across the surface. The N-terminal helix inside the pore that stabilizes the barrel is unaffected by the binding of mNT, suggesting that mNT does not bind deep enough into the barrel to alter exchange within this region, which still exchanges freely with solvent. Notably, peptides with increased protection upon complex formation extend down the side of the VDAC barrel, opposite the internal helical region. These observed changes in exchange protection may indicate that mNT forms contacts further down the side of the barrel opposite the internal helix, or

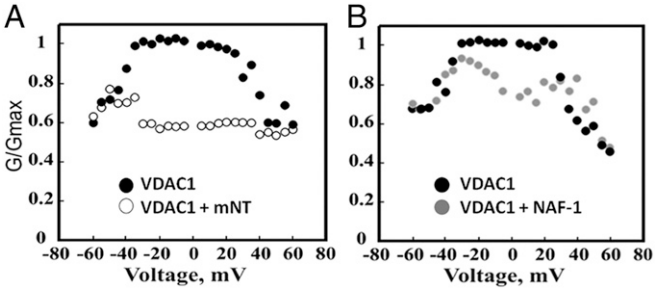

Fig. 2. VDAC channel conductance is inhibited by mNT. VDAC was reconstituted into a planar lipid bilayer and channel conductance was measured as a function of applied voltage. The recordings were taken before and after the addition of 5 μg/mL mNT (*A*) or NAF-1 (*B*). Conductance measurements were normalized to the conductance at 10 mV using the following formula: G/G_{max} = (Conductance/Maximal Conductance of Control).

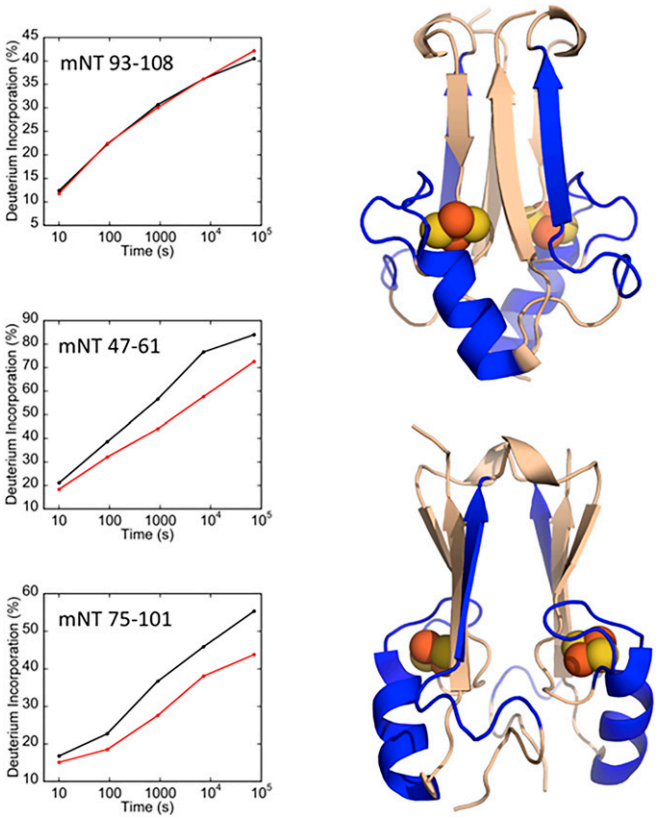

Fig. 3. Regions of mNT with increased protection upon interaction with VDAC. Selected plots of deuterium incorporation into peptides from regions with significant increases in protection upon complex formation are shown. An additional plot is given (peptide 93 to 108) that is representative of a region with no significant change in deuterium incorporation upon complex formation. Regions that exhibit significant increases in HD-exchange protection are highlighted on the mNT crystal structure (PDB ID code 2QH7) in blue, while regions with similar protection factors are shown in beige.

that changes in local motions from binding are extended down the barrel wall. Taken together, these data indicate that mNT binds across the cytosolic side of the VDAC channel and partially into the barrel.

In investigations independent of the HDX-MS experiments, we performed computational docking analysis of the 2 proteins (*SI Appendix*, Fig. S4). In the final docked complex, mNT fits asymmetrically into the VDAC channel with one mNT [2Fe-2S] cluster-binding domain contacting the cytosolic loops of VDAC, above the N-terminal helix. The β-cap of mNT is positioned in between the N-terminal helix (but not contacting it) and diametrically opposed to the helix barrel wall of VDAC. This docked model matches well with our experimental data, supporting a likely mode of protein–protein interaction.

The VDAC Inhibitor DIDS Prevents Both mNT–VDAC Binding and Influences Iron/Fe-S Flux between mNT and the Mitochondria. The binding of mNT and VDAC in vitro was interrogated in the presence of a known inhibitor of VDAC channels, with MST analysis. Fluorescently labeled VDAC in phospholipid bicelles was pretreated with DIDS followed by MST analysis of mNT binding. The presence of DIDS completely prevented detectable binding of mNT to VDAC (Fig. 5*A*) while not affecting the redox state of mNT (*SI Appendix*, Fig. S5). Given this observation, we then determined whether inhibiting the interaction would prevent the transfer of iron into the mitochondria in situ, as we previously discovered that addition of oxidized mNT to gently permeabilized cells results in influx of iron into the mitochondria (2). Soluble mNT was added to gently permeabilized h9c2 cells. Rhodamine B-[(1,10-phenanthrolin-5-yl)-aminocarbonyl] benzyl ester (RPA) was used as an indicator of mitochondrial iron. We monitored the change in fluorescence in response to addition of mNT in situ. RPA is rapidly quenched following addition of mNT, indicating transfer of iron into mitochondria. Although these studies are not under physiological conditions, they demonstrate that mNT binding to VDAC can also occur within the cellular environment (Fig. 5*B*). Notably, in the presence of the VDAC inhibitor DIDS, the quenching of RPA is significantly reduced (Fig. 5*B*).

Fig. 6 reconciles all experimental and computational analyses to create a representative model of the complexed mNT and VDAC proteins. VDAC transports metabolites, such as ATP, ADP, pyruvate, and fatty acids, across the OMM between the cytosol and intermembrane space. One effect of VDAC closure is inhibited fatty acid metabolism in the mitochondria, leading to lipid accumulation in the cytosol. Fatty liver disease (liver steatosis) and chronic ethanol exposure are associated with insulin resistance (53, 54), while insulin resistance and alcohol metabolism are also associated with oxidative stress (55, 56). A recent study demonstrated that the genetic knockout of mNT prevented liver steatosis in ethanol-fed mice (57). Moreover, exposure to

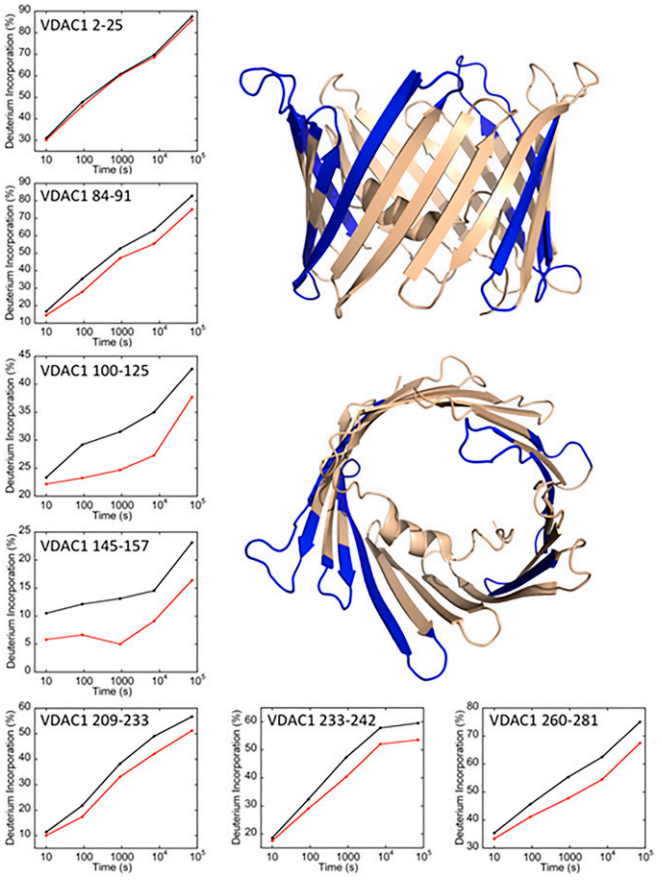

Fig. 4. Regions of VDAC with increased protection upon interaction with mNT. Selected plots of deuterium incorporation into peptides from regions with significant increases in protection upon complex formation are shown. An additional plot is given (peptide 2 to 25) that is representative of peptides with no significant change in deuterium incorporation upon complex formation. This unaffected peptide corresponds to the N-terminal α-helix inside the VDAC barrel. Regions that exhibit significant increases in HD-exchange protection are highlighted on the VDAC crystal structure (PDB ID code 5XDO) in blue, and those without changes are in beige.

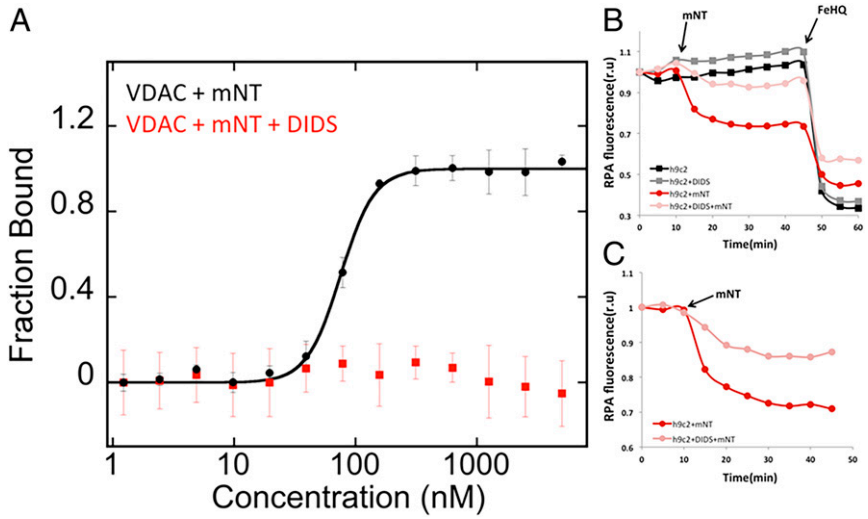

Fig. 5. DIDS inhibits mNT–VDAC interaction. (*A*) MST analysis of the effect of DIDS on the binding of mNT to fluorescently labeled VDAC in 1% DMPC/CHAPSO bicelles under oxidizing conditions. The final DIDS concentration following mNT addition was 700 μM. (*B* and *C*) The effect of DIDS on mNT-induced changes in mitochondrial iron levels. H9c2 cells were preincubated with and without DIDS (100 μM) for 1 h, labeled with RPA, and permeabilized with digitonin to allow the entry of mNT into cells. The change in RPA fluorescence was followed every 5 min. Twenty micromolar mNT was added after 10 min. Five micromolar ferrous ammonium sulfate, complexed to equimolar hydroxyquinoline (FeHQ), which is a siderophore that allows iron to pass the membrane, was added after 45 min. RPA fluorescence is expressed in relative units (r.u.) obtained by analyzing individual cell fluorescence with ImageJ (open software), by averaging 5 cells per field.

ethanol induces a decrease in mitochondrial function via VDAC closure (58). This effect results in a reduction of mitochondrial ATP production, as well as in inhibition of fatty acid oxidation (58). We have shown with perturbation studies that soluble mNT added to permeabilized cells could transfer its Fe/[2Fe-2S] cluster directly into the mitochondria (1, 2). We now show that addition of the VDAC inhibitor DIDS prevents the mitochondrial Fe/[2Fe-2S] accumulation with the addition of soluble mNT, indicating that the interaction with VDAC provides one conduit for this transfer. Our results suggest that, under oxidative stress that could be induced by different sources, VDAC channels are blocked by binding of oxidized mNT with nanomolar affinity and this binding limits channel conductance by favoring the closed state of the channel. Binding of the type 2 diabetes drug pioglitazone stabilizes the oxidized [2Fe-2S] cluster against release (16) and could inhibit the transfer of iron into the mitochondria (21). However, it must be stated that pioglitazone binding can cause a bottleneck in cytosol/mitochondrial cross talk and also inhibit the biologically relevant transfer of iron out of the mitochondria and promote ROS accumulation as we have shown in cancer cells (5).

Because mNT has a redox-active [2Fe-2S] cluster, is linked to the glutathione system, and protects cardiomyocytes from oxidative-stress–mediated apoptosis, it may have a role in cellular redox sensing (16, 21, 59, 60). This idea is further supported by a number of studies showing that mNT's [2Fe-2S] cluster transfer occurs in the more labile, oxidized state (12, 21, 61, 62). Therefore, it is perhaps unsurprising that only oxidized mNT binds VDAC. However, cell death, stress, or defense conditions can change the cellular redox state, through ROS by-products of disrupted oxidative phosphorylation, leading to a reduction of the [2Fe-2S] clusters in mNT (45, 63–65). Such redox-dependent binding supports a proposal that the [2Fe -2S] clusters of mNT act as an on/off switch accompanied by profound alterations of its protein interactions and cellular function. With the mitochondria being the largest source of superoxide and other ROS in the cell, mNT is in ideal proximity for redox sensing and cytosolic communication due to its strategic location on the OMM facing the cytosol (66–69). Our results establish an important interaction between mNT and VDAC in the OMM that occurs under oxidative conditions. This interaction is potentially part of a stress response that can result in cell death by ferroptosis and may also be a potential source of mitochondrial iron overload during oxidative stress (6, 54, 70).

Materials and Methods

Expression and Purification of Human mNT and VDAC. Human mNT was expressed and purified as described (21). Recombinant human VDAC with a C-terminal 6×His tag was expressed as described (71). Nanodiscs containing VDAC were prepared using the covalently circularized cNW9 scaffold protein and DMPC/DMPG at a 3:1 ratio as described (72).

MST. Purified VDAC was fluorescently labeled using the amine reactive RED-NHS NT-647 dye (NanoTemper) according to the manufacturer's protocol, and was studied both in lipid bicelles as well as covalently circularized nanodiscs (cND)

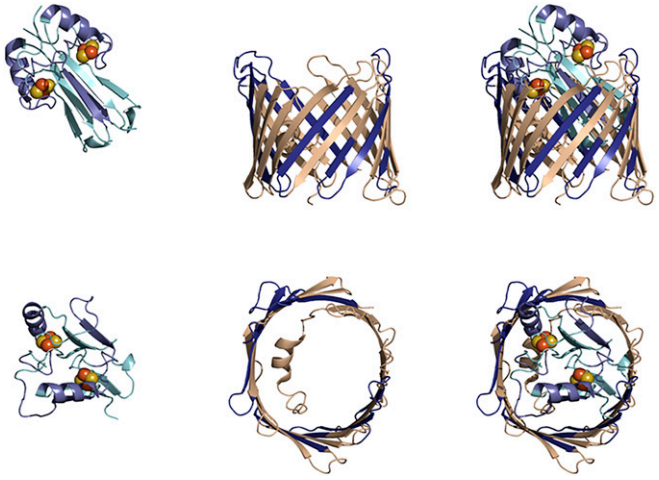

Fig. 6. Combined experimental and computational model of mNT docked to VDAC. Data from HDX-MS experiments and Fd-DCA calculations were combined to generate a model for the docking of the mNT dimer inside the VDAC pore. Increased protection mapping is indicated by darker blues, minimal protection by light blues, and no protection by tan. VDAC PDB ID code, 5XDO; MNT PDB ID code, 2QH7.

(72). The DMPC/CHAPSO (3:1) bicelle mixture was added to the fluorescently labeled VDAC (in lauryldimethylamine oxide [LDAO] micelles) to a concentration of 2% and incubated on ice for 30 min. The VDAC-bicelle mixture was diluted to 50 nM in 50 mM phosphate buffer, 100 mM NaCl, 2% bicelles, pH 7.0. VDAC was also assembled in the cNDs recently described by Nasr et al. (72), which incorporates a single VDAC protein in each nanodisc. Nanodiscs containing VDAC were fluorescently labeled in lipid bicelles, in the same manner as described above. MST analysis was performed at 22 °C using a Monolith NT.115 system (NanoTemper) using a constant concentration of labeled VDAC in either bicelles or nanodiscs and a 1:1 serial dilution of mNT in 50 mM sodium phosphate, 100 mM NaCl, pH 7.0. MST analysis of VDAC bicelles with reduced mNT was performed in the same buffer at pH 8.0 with the addition of 20 mM DTT. Replicate MST measurements were collected for all VDAC-bicelle and VDAC-nanodiscs mNT binding studies. Small-molecule inhibitor binding of DIDS was performed with preincubation of VDAC with a DIDS concentration of 700 μM (the 10-fold concentration above the 70 μM K_D of VDAC with DIDS reflects conditions where 99.9% of VDAC is bound with DIDS).

Data were normalized and fit to the Hill equation with a Hill coefficient >1 using KaleidaGraph software (Synergy Software).

Gating Experiments. VDAC from sheep liver mitochondria was solubilized with LDAO and purified using hydroxyapatite resin as described previously (73). The purified VDAC was used for channel reconstitution into a planar lipid bilayer. Sheep liver were chosen as the source for VDAC as it exhibits 99.3% sequence identity with the human protein (74) (*SI Appendix*, Fig. S6). VDAC was added to the patch clamp *cis* chamber containing 0.5 M NaCl and 10 mM Hepes, pH 7.4. After one or more channels were inserted into the planar lipid bilayer, currents were recorded by voltage clamping using a Bilayer Clamp BC-525B amplifier (Warner Instruments). Current was measured with respect to the *trans* side of the membrane (ground) in the presence and absence of purified mNT and NAF-1. The current was digitized on-line using a Digidata 1200 interface board and pCLAMP 6 software (Axon Instruments).

Cellular Studies. Given the observation that DIDS inhibits the binding of mNT to VDAC in vitro, we then determined whether inhibiting the interaction would prevent the transfer of iron into the mitochondria in situ. As we previously discovered via perturbation studies, the addition of oxidized mNT to gently permeabilized cells results in an influx of iron into the mitochondria (21). Soluble, oxidized mNT was added to gently permeabilized h9c2 cells. Using RPA as an indicator of mitochondrial iron, we monitored the change in fluorescence in response to addition of mNT.

Stability Analysis. The potential effect of the lipids and interaction of VDAC on the cluster stability mNT was assessed following the absorption of the [2Fe-2S] clusters over time as described previously (2, 15, 16, 70, 75). Briefly, 25 μM mNT was incubated in the presence of 25 μM empty nanodiscs (negative control) as well as 25 μM nanodiscs containing VDAC in 50 mM sodium phosphate, 100 mM NaCl, pH 7.0, at 37 °C. The absorbance at 458 nm was monitored as a function of time as previously published (12, 62, 70, 76).

HDX-MS. To elucidate the regions important for the interactions between oxidized mNT and VDAC, we first determined the optimum conditions for final mass spectral analysis of HDX-MS. In an effort to get the maximum coverage of both proteins, we explored a range of denaturant conditions, proteases, and pHs for final analysis as described (77–83). Our HDX experiments were carried out in 10 mM sodium phosphate, 100 mM NaCl, pH 7.0, with a final D_2O concentration of 90%. The hydrogen–deuterium exchange reaction was quenched at 4 °C with a final concentration of 500 mM guanidine-HCl, 0.5% formic acid, and 10% glycerol in D_2O and flash frozen. Samples were stored at −80 °C until analyzed. Instrument setup and operation were described previously (84). Both porcine pepsin and fungal protease XIII were used to enhance peptide coverage. Peptides were identified using Sequest software (Thermo Finnigan). Each peptide was evaluated at every time point for quality control. Deuterium content for each time point was calculated using DXMS Explorer (Sierra Analytics).

Computational Methodology. Our protein–protein binding site identification method, Fd-DCA (fragment docking–direct coupling analysis), was used to predict the highest probability mNT–VDAC binding sites from coevolving residues (85). These residue–residue couplings were taken as constraints for modeling the initial energetically favorable binding complex of mNT–VDAC (83). I-TASSER was used to model the N-terminal transmembrane domain (residues 14 to 31) of mNT as an α-helix, since it was not available in the crystal structure (86). Then the modeled molecular structure of mNT was explored to identify candidate binding sites for protein–protein interaction. As a result, 3 sites were obtained, as shown in *SI Appendix*, Fig. S7. The largest binding site, designated as site 1, covers the 2Fe-2S cluster region. Site 2 is adjacent to the membrane domain, and site 3 is relatively small and located in the β-cap domain, under site 1. To discriminate which binding site of mNT interacts with VDAC, DCA was performed between mNT and VDAC. The sequences of mNT were collected from UniProt (13, 87). The sequence alignment of VDAC was obtained from Jackhmmer (88) by using the fast sequence of the Protein Data Bank (PDB) entry (5XDO) of VDAC as the template. To join these 2 sequence alignments, we followed the same rules presented in our previous work (85). The predicted top 20 coevolving residue pairs between the 2 proteins are listed in *SI Appendix*, Table S1. Interestingly, a part of these coevolving signals are across the soluble domain of mNT and VDAC, and the other part is from the membrane domain of mNT and VDAC. Meanwhile, as shown in *SI Appendix*, Table S1 and Fig. S3, these predicted coevolving residues of mNT are largely overlapped with the residues on identified site 1 and site 2. This indicated that VDAC could interact with both binding sites of mNT. Taking these top 20 coevolving residue pairs as the constraints, we docked mNT into VDAC to create a binding complex and used a Steepest Descent (SD) energy minimization from Gromacs v5.0.5MD to optimize a final, complex structure, shown in *SI Appendix*, Fig. S8.

ACKNOWLEDGMENTS. This work was supported by NSF–Binational Science Foundation (BSF) funding (NSF-MCB-1613462 [R.M.]) and BSF (BSF Grant 2015831 [R.N.]). Work at the laboratory of P.A.J. is supported by National Institutes of Health Grant GM101467. J.N.O. is a Cancer Prevention and Research Institute of Texas (CPRIT) Scholar in Cancer Research sponsored by CPRIT. J.N.O. was supported by the Center for Theoretical Biological Physics sponsored by the NSF (Grant PHY-1427654) and by NSF-CHE 1614101. The funders had no role in the design, data collection, analysis, decision to publish, or preparation of the manuscript. We also thank Prof. Varda Shoshan-Barmatz from Ben Gurion University, who generously shared her VDAC conducting system to collect data that was used in Fig. 2, as well as Prof. Emmanuel Theodorakis and Dr. Kendra Hailey from University of California at San Diego for their thoughtful as well as valuable insights into this manuscript.

1. R. Nechushtai *et al.*, Characterization of *Arabidopsis* NEET reveals an ancient role for NEET proteins in iron metabolism. *Plant Cell* **24**, 2139–2154 (2012).
2. S. Tamir *et al.*, Structure-function analysis of NEET proteins uncovers their role as key regulators of iron and ROS homeostasis in health and disease. *Biochim. Biophys. Acta* **1853**, 1294–1315 (2015).
3. H. Yuan, X. Li, X. Zhang, R. Kang, D. Tang, CISD1 inhibits ferroptosis by protection against mitochondrial lipid peroxidation. *Biochem. Biophys. Res. Commun.* **478**, 838–844 (2016).
4. J. R. Colca *et al.*, Identification of a novel mitochondrial protein ("mitoNEET") cross-linked specifically by a thiazolidinedione photoprobe. *Am. J. Physiol. Endocrinol. Metab.* **286**, E252–E260 (2004).
5. M. Darash-Yahana *et al.*, Breast cancer tumorigenicity is dependent on high expression levels of NAF-1 and the lability of its Fe-S clusters. *Proc. Natl. Acad. Sci. U.S.A.* **113**, 10890–10895 (2016).
6. Y. S. Sohn *et al.*, NAF-1 and mitoNEET are central to human breast cancer proliferation by maintaining mitochondrial homeostasis and promoting tumor growth. *Proc. Natl. Acad. Sci. U.S.A.* **110**, 14676–14681 (2013).
7. S. Amr *et al.*, A homozygous mutation in a novel zinc-finger protein, ERIS, is responsible for Wolfram syndrome 2. *Am. J. Hum. Genet.* **81**, 673–683 (2007).
8. G. L. Taminelli *et al.*, CISD1 codifies a mitochondrial protein upregulated by the CFTR channel. *Biochem. Biophys. Res. Commun.* **365**, 856–862 (2008).
9. Y. F. Chen *et al.*, Cisd2 deficiency drives premature aging and causes mitochondria-mediated defects in mice. *Genes Dev.* **23**, 1183–1194 (2009).
10. C. M. Kusminski *et al.*, MitoNEET-driven alterations in adipocyte mitochondrial activity reveal a crucial adaptive process that preserves insulin sensitivity in obesity. *Nat. Med.* **18**, 1539–1549 (2012).
11. W. J. Geldenhuys, T. C. Leeper, R. T. Carroll, mitoNEET as a novel drug target for mitochondrial dysfunction. *Drug Discov. Today* **19**, 1601–1606 (2014).
12. S. E. Wiley, A. N. Murphy, S. A. Ross, P. van der Geer, J. E. Dixon, MitoNEET is an iron-containing outer mitochondrial membrane protein that regulates oxidative capacity. *Proc. Natl. Acad. Sci. U.S.A.* **104**, 5318–5323 (2007).
13. S. Sengupta *et al.*, Phylogenetic analysis of the CDGSH iron-sulfur binding domain reveals its ancient origin. *Sci. Rep.* **8**, 4840 (2018).
14. M. A. Inupakutika *et al.*, Phylogenetic analysis of eukaryotic NEET proteins uncovers a link between a key gene duplication event and the evolution of vertebrates. *Sci. Rep.* **7**, 42571 (2017).
15. S. E. Wiley *et al.*, The outer mitochondrial membrane protein mitoNEET contains a novel redox-active 2Fe-2S cluster. *J. Biol. Chem.* **282**, 23745–23749 (2007).
16. M. L. Paddock *et al.*, MitoNEET is a uniquely folded 2Fe 2S outer mitochondrial membrane protein stabilized by pioglitazone. *Proc. Natl. Acad. Sci. U.S.A.* **104**, 14342–14347 (2007).
17. J. Lin, T. Zhou, K. Ye, J. Wang, Crystal structure of human mitoNEET reveals distinct groups of iron sulfur proteins. *Proc. Natl. Acad. Sci. U.S.A.* **104**, 14640–14645 (2007).

18. X. Hou *et al*., Crystallographic studies of human MitoNEET. *J. Biol. Chem.* **282**, 33242–33246 (2007).
19. I. Ferecatu *et al*., The diabetes drug target MitoNEET governs a novel trafficking pathway to rebuild an Fe-S cluster into cytosolic aconitase/iron regulatory protein 1. *J. Biol. Chem.* **289**, 28070–28086 (2014).
20. S. Tamir *et al*., Nutrient-deprivation autophagy factor-1 (NAF-1): Biochemical properties of a novel cellular target for anti-diabetic drugs. *PLoS One* **8**, e61202 (2013).
21. J. A. Zuris *et al*., Facile transfer of [2Fe-2S] clusters from the diabetes drug target mitoNEET to an apo-acceptor protein. *Proc. Natl. Acad. Sci. U.S.A.* **108**, 13047–13052 (2011).
22. C. H. Lipper *et al*., Cancer-related NEET proteins transfer 2Fe-2S clusters to anamorsin, a protein required for cytosolic iron-sulfur cluster biogenesis. *PLoS One* **10**, e0139699 (2015).
23. J. J. Lemasters, E. Holmuhamedov, Voltage-dependent anion channel (VDAC) as mitochondrial governator—thinking outside the box. *Biochim. Biophys. Acta* **1762**, 181–190 (2006).
24. V. Shoshan-Barmatz *et al*., VDAC, a multi-functional mitochondrial protein regulating cell life and death. *Mol. Aspects Med.* **31**, 227–285 (2010).
25. K. Fukada, F. Zhang, A. Vien, N. R. Cashman, H. Zhu, Mitochondrial proteomic analysis of a cell line model of familial amyotrophic lateral sclerosis. *Mol. Cell. Proteomics* **3**, 1211–1223 (2004).
26. P. H. Reddy, Is the mitochondrial outer membrane protein VDAC1 therapeutic target for Alzheimer's disease? *Biochim. Biophys. Acta* **1832**, 67–75 (2013).
27. A. Smilansky *et al*., The voltage-dependent anion channel 1 mediates amyloid β toxicity and represents a potential target for Alzheimer disease therapy. *J. Biol. Chem.* **290**, 30670–30683 (2015).
28. V. Shoshan-Barmatz, E. Nahon-Crystal, A. Shteinfer-Kuzmine, R. Gupta, VDAC1, mitochondrial dysfunction, and Alzheimer's disease. *Pharmacol. Res.* **131**, 87–101 (2018).
29. M. Manczak, T. Sheiko, W. J. Craigen, P. H. Reddy, Reduced VDAC1 protects against Alzheimer's disease, mitochondria, and synaptic deficiencies. *J. Alzheimers Dis.* **37**, 679–690 (2013).
30. A. Tikunov *et al*., Closure of VDAC causes oxidative stress and accelerates the Ca^{2+}-induced mitochondrial permeability transition in rat liver mitochondria. *Arch. Biochem. Biophys.* **495**, 174–181 (2010).
31. D. Fang, E. N. Maldonado, VDAC regulation: A mitochondrial target to stop cell proliferation. *Adv. Cancer Res.* **138**, 41–69 (2018).
32. J. Gatliff *et al*., TSPO interacts with VDAC1 and triggers a ROS-mediated inhibition of mitochondrial quality control. *Autophagy* **10**, 2279–2296 (2014).
33. E. N. Maldonado *et al*., Voltage-dependent anion channels modulate mitochondrial metabolism in cancer cells: Regulation by free tubulin and erastin. *J. Biol. Chem.* **288**, 11920–11929 (2013).
34. A. Messina, S. Reina, F. Guarino, V. De Pinto, VDAC isoforms in mammals. *Biochim. Biophys. Acta* **1818**, 1466–1476 (2012).
35. M. J. Sampson, R. S. Lovell, W. J. Craigen, The murine voltage-dependent anion channel gene family. Conserved structure and function. *J. Biol. Chem.* **272**, 18966–18973 (1997).
36. C. Wan *et al*., Panorama of ancient metazoan macromolecular complexes. *Nature* **525**, 339–344 (2015).
37. K. G. Guruharsha *et al*., A protein complex network of *Drosophila melanogaster*. *Cell* **147**, 690–703 (2011).
38. R. Benz, Permeation of hydrophilic solutes through mitochondrial outer membranes: Review on mitochondrial porins. *Biochim. Biophys. Acta* **1197**, 167–196 (1994).
39. S. J. Schein, M. Colombini, A. Finkelstein, Reconstitution in planar lipid bilayers of a voltage-dependent anion-selective channel obtained from paramecium mitochondria. *J. Membr. Biol.* **30**, 99–120 (1976).
40. E. Pavlov *et al*., The mitochondrial channel VDAC has a cation-selective open state. *Biochim. Biophys. Acta* **1710**, 96–102 (2005).
41. V. De Pinto *et al*., Characterization of human VDAC isoforms: A peculiar function for VDAC3? *Biochim. Biophys. Acta* **1797**, 1268–1275 (2010).
42. V. Shoshan-Barmatz *et al*., VDAC/porin is present in sarcoplasmic reticulum from skeletal muscle. *FEBS Lett.* **386**, 205–210 (1996).
43. H. Flörke *et al*., Channel active mammalian porin, purified from crude membrane fractions of human B lymphocytes and bovine skeletal muscle, reversibly binds adenosine triphosphate (ATP). *Biol. Chem. Hoppe Seyler* **375**, 513–520 (1994).
44. D. W. Bak, J. A. Zuris, M. L. Paddock, P. A. Jennings, S. J. Elliott, Redox characterization of the FeS protein MitoNEET and impact of thiazolidinedione drug binding. *Biochemistry* **48**, 10193–10195 (2009).
45. Y. Wang, A. P. Landry, H. Ding, The mitochondrial outer membrane protein mitoNEET is a redox enzyme catalyzing electron transfer from $FMNH_2$ to oxygen or ubiquinone. *J. Biol. Chem.* **292**, 10061–10067 (2017).
46. J. A. Zuris *et al*., Engineering the redox potential over a wide range within a new class of FeS proteins. *J. Am. Chem. Soc.* **132**, 13120–13122 (2010).
47. D. W. Bak, S. J. Elliott, Alternative FeS cluster ligands: Tuning redox potentials and chemistry. *Curr. Opin. Chem. Biol.* **19**, 50–58 (2014).
48. T. K. Rostovtseva, S. M. Bezrukov, VDAC regulation: Role of cytosolic proteins and mitochondrial lipids. *J. Bioenerg. Biomembr.* **40**, 163–170 (2008).
49. T. K. Rostovtseva, S. M. Bezrukov, VDAC inhibition by tubulin and its physiological implications. *Biochim. Biophys. Acta* **1818**, 1526–1535 (2012).
50. H. Azoulay-Zohar, A. Israelson, S. Abu-Hamad, V. Shoshan-Barmatz, In self-defence: Hexokinase promotes voltage-dependent anion channel closure and prevents mitochondria-mediated apoptotic cell death. *Biochem. J.* **377**, 347–355 (2004).
51. M. Colombini, A candidate for the permeability pathway of the outer mitochondrial membrane. *Nature* **279**, 643–645 (1979).
52. Y. Tsutsui, P. L. Wintrode, Hydrogen/deuterium exchange-mass spectrometry: A powerful tool for probing protein structure, dynamics and interactions. *Curr. Med. Chem.* **14**, 2344–2358 (2007).
53. M. Gaggini *et al*., Non-alcoholic fatty liver disease (NAFLD) and its connection with insulin resistance, dyslipidemia, atherosclerosis and coronary heart disease. *Nutrients* **5**, 1544–1560 (2013).
54. C. S. Lieber, Alcoholic fatty liver: Its pathogenesis and mechanism of progression to inflammation and fibrosis. *Alcohol* **34**, 9–19 (2004).
55. T. Zima *et al*., Oxidative stress, metabolism of ethanol and alcohol-related diseases. *J. Biomed. Sci.* **8**, 59–70 (2001).
56. J. L. Evans, I. D. Goldfine, B. A. Maddux, G. M. Grodsky, Are oxidative stress-activated signaling pathways mediators of insulin resistance and beta-cell dysfunction? *Diabetes* **52**, 1–8 (2003).
57. X. Hu *et al*., MitoNEET deficiency alleviates experimental alcoholic steatohepatitis in mice by stimulating endocrine adiponectin-fgf15 axis. *J. Biol. Chem.* **291**, 22482–22495 (2016).
58. E. Holmuhamedov, J. J. Lemasters, Ethanol exposure decreases mitochondrial outer membrane permeability in cultured rat hepatocytes. *Arch. Biochem. Biophys.* **481**, 226–233 (2009).
59. A. Habener *et al*., MitoNEET protects HL-1 cardiomyocytes from oxidative stress mediated apoptosis in an in vitro model of hypoxia and reoxygenation. *PLoS One* **11**, e0156054 (2016).
60. C. Mons *et al*., The H_2O_2-resistant Fe-S redox switch MitoNEET acts as a pH sensor to repair stress-damaged Fe-S protein. *Biochemistry* **57**, 5616–5628 (2018).
61. M. P. Golinelli-Cohen *et al*., Redox control of the human iron-sulfur repair protein MitoNEET activity via its iron-sulfur cluster. *J. Biol. Chem.* **291**, 7583–7593 (2016).
62. A. R. Conlan *et al*., Mutation of the His ligand in mitoNEET stabilizes the 2Fe-2S cluster despite conformational heterogeneity in the ligand environment. *Acta Crystallogr. D Biol. Crystallogr.* **67**, 516–523 (2011).
63. X. Y. Chen *et al*., Isoliquiritigenin induces mitochondrial dysfunction and apoptosis by inhibiting mitoNEET in a reactive oxygen species-dependent manner in A375 human melanoma cells. *Oxid. Med. Cell. Longev.* **2019**, 9817576 (2019).
64. A. P. Landry, Z. Cheng, H. Ding, Reduction of mitochondrial protein mitoNEET [2Fe-2S] clusters by human glutathione reductase. *Free Radic. Biol. Med.* **81**, 119–127 (2015).
65. A. P. Landry, H. Ding, Redox control of human mitochondrial outer membrane protein MitoNEET [2Fe-2S] clusters by biological thiols and hydrogen peroxide. *J. Biol. Chem.* **289**, 4307–4315 (2014).
66. J. F. Turrens, Mitochondrial formation of reactive oxygen species. *J. Physiol.* **552**, 335–344 (2003).
67. M. P. Murphy, How mitochondria produce reactive oxygen species. *Biochem. J.* **417**, 1–13 (2009).
68. A. Phaniendra, D. B. Jestadi, L. Periyasamy, Free radicals: Properties, sources, targets, and their implication in various diseases. *Indian J. Clin. Biochem.* **30**, 11–26 (2015).
69. L. A. Pham-Huy, H. He, C. Pham-Huy, Free radicals, antioxidants in disease and health. *Int. J. Biomed. Sci.* **4**, 89–96 (2008).
70. F. Bai *et al*., The Fe-S cluster-containing NEET proteins mitoNEET and NAF-1 as chemotherapeutic targets in breast cancer. *Proc. Natl. Acad. Sci. U.S.A.* **112**, 3698–3703 (2015).
71. T. J. Malia, G. Wagner, NMR structural investigation of the mitochondrial outer membrane protein VDAC and its interaction with antiapoptotic Bcl-xL. *Biochemistry* **46**, 514–525 (2007).
72. M. L. Nasr *et al*., Covalently circularized nanodiscs for studying membrane proteins and viral entry. *Nat. Methods* **14**, 49–52 (2017).
73. D. Ben-Hail, V. Shoshan-Barmatz, Purification of VDAC1 from rat liver mitochondria. *Cold Spring Harb. Protoc.* **2014**, 94–99 (2014).
74. S. F. Altschul, W. Gish, W. Miller, E. W. Myers, D. J. Lipman, Basic local alignment search tool. *J. Mol. Biol.* **215**, 403–410 (1990).
75. E. L. Baxter *et al*., Allosteric control in a metalloprotein dramatically alters function. *Proc. Natl. Acad. Sci. U.S.A.* **110**, 948–953 (2013).
76. J. A. Zuris *et al*., NADPH inhibits [2Fe-2S] cluster protein transfer from diabetes drug target MitoNEET to an apo-acceptor protein. *J. Biol. Chem.* **287**, 11649–11655 (2012).
77. B. E. Aubol, K. L. Hailey, L. Fattet, P. A. Jennings, J. A. Adams, Redirecting SR protein nuclear trafficking through an allosteric platform. *J. Mol. Biol.* **429**, 2178–2191 (2017).
78. K. M. Fisher *et al*., Geometrical frustration in interleukin-33 decouples the dynamics of the functional element from the folding transition state ensemble. *PLoS One* **10**, e0144067 (2015).
79. K. L. Hailey, D. T. Capraro, S. Barkho, P. A. Jennings, Allosteric switching of agonist/antagonist activity by a single point mutation in the interluekin-1 receptor antagonist, IL-1Ra. *J. Mol. Biol.* **425**, 2382–2392 (2013).
80. K. L. Hailey *et al*., Pro-interleukin (IL)-1beta shares a core region of stability as compared with mature IL-1beta while maintaining a distinctly different configurational landscape: A comparative hydrogen/deuterium exchange mass spectrometry study. *J. Biol. Chem.* **284**, 26137–26148 (2009).
81. M. M. Keshwani *et al*., Nuclear protein kinase CLK1 uses a non-traditional docking mechanism to select physiological substrates. *Biochem. J.* **472**, 329–338 (2015).
82. R. M. Plocinik *et al*., Regulating SR protein phosphorylation through regions outside the kinase domain of SRPK1. *J. Mol. Biol.* **410**, 131–145 (2011). Erratum in: *J. Mol. Biol.* **411**, 511 (2011).
83. S. Tamir *et al*., Integrated strategy reveals the protein interface between cancer targets Bcl-2 and NAF-1. *Proc. Natl. Acad. Sci. U.S.A.* **111**, 5177–5182 (2014).
84. S. Barkho *et al*., Distal loop flexibility of a regulatory domain modulates dynamics and activity of C-terminal SRC kinase (csk). *PLoS Comput. Biol.* **9**, e1003188 (2013).
85. F. Bai, F. Morcos, R. R. Cheng, H. Jiang, J. N. Onuchic, Elucidating the druggable interface of protein-protein interactions using fragment docking and coevolutionary analysis. *Proc. Natl. Acad. Sci. U.S.A.* **113**, E8051–E8058 (2016).
86. J. Yang *et al*., The I-TASSER suite: Protein structure and function prediction. *Nat. Methods* **12**, 7–8 (2015).
87. A. Perrier-Cornet *et al*., Decreased turnover aspirin resistance by bidaily aspirin intake and efficient cytoreduction in myeloproliferative neoplasms. *Platelets* **29**, 723–728 (2018).
88. R.D. Finn *et al*., HMMER web server: 2015 update. *Nucleic Acids Res.* **43**, W30–W38 (2015).